

Elastic magnetic electron scattering from ^{41}Ca

H. Baghaei,⁽¹⁾ A. Cichocki,⁽¹⁾ J. B. Flanz,⁽²⁾ M. Frodyma,^{(1)*} B. Frois,⁽³⁾ Y. Han,^{(1)†}
 R. S. Hicks,⁽¹⁾ J. Martino,⁽³⁾ R. A. Miskimen,⁽¹⁾ C. N. Papanicolas,⁽⁴⁾ G. A. Peterson,⁽¹⁾ S. Platchkov,⁽³⁾ S. Raman,⁽⁵⁾
 S. H. Rokni,^{(1)‡} and T. Suzuki⁽⁶⁾

⁽¹⁾*Department of Physics and Astronomy, University of Massachusetts, Amherst, Massachusetts 01003*

⁽²⁾*Massachusetts Institute of Technology—Bates Linear Accelerator Center, Middelton, Massachusetts 01949*

⁽³⁾*Centre d'Etudes Nucléaires Saclay, F-91191 Gif-sur-Yvette, France*

⁽⁴⁾*Department of Physics, University of Illinois, Champaign, Illinois 61820*

⁽⁵⁾*Oak Ridge National Laboratory, Oak Ridge, Tennessee 37831*

⁽⁶⁾*Department of Physics, Nihon University, Tokyo, Japan*

(Received 16 July 1990)

The elastic magnetic form factor of ^{41}Ca has been determined by 180° electron scattering in the momentum-transfer range $0.9\text{--}2.0\text{ fm}^{-1}$. An analysis of the data indicates that the amplitudes of the $M3$ and $M5$ multipoles are quenched by factors of 0.57 ± 0.16 and 0.68 ± 0.07 relative to the simple shell model. In contrast, the magnitude of the $M7$ form factor is in good accord with this model. Calculations that include multiparticle-multihole configurations in the $1f_{7/2}$ and $1d_{3/2}$ subshells, first-order core polarization to higher excited orbitals, and meson exchange currents give reasonable agreement with the data for all multipoles. The rms radius of the $1f_{7/2}$ neutron orbit was determined by means of a combined analysis of our results and previous data obtained at higher momentum transfers. After correcting for core polarization and meson exchange currents, the radius was found to be $3.96\pm 0.05\text{ fm}$, in agreement with the predictions of mean-field calculations.

I. INTRODUCTION

Elastic electron scattering is a powerful technique for determining the ground-state charge and current distributions of nuclei. Coulomb electron scattering has been utilized to determine precise and detailed nuclear charge distributions, and magnetic electron scattering has provided information on nuclear current distributions. According to the shell model, nuclear magnetism is determined by valence nucleons. Therefore, magnetic electron scattering gives insight into the single-particle aspects of the nucleus. Such scattering can arise from interactions with not only orbital currents but also spin currents, and so can be used to study the single-particle wave functions of both neutrons and protons.

Elastic magnetic form factors¹ have been measured over a broad range of momentum transfer for a large number of nuclei, ranging from ^1H to ^{209}Bi . Although the independent-particle model describes the qualitative features of these data, the form factor magnitudes are not usually well reproduced. In particular, for the momentum transfer region $q \lesssim 2\text{ fm}^{-1}$, where low and intermediate magnetic multipoles are dominant, single-particle calculations tend to exceed the data. Furthermore, smaller discrepancies have been observed at larger momentum transfers where the highest magnetic multipole is dominant. Such disagreements have been interpreted in terms of core polarization (CP), meson-exchange currents (ME's), Δ -isobar excitation, and relativistic effects.

The interpretation of magnetic form factors is simpler for nuclei that have a single nucleon outside a doubly closed core,¹ especially if the nucleon is in a "stretched"

configuration, $j = l + \frac{1}{2}$. According to the single-particle picture, the q dependence of the highest magnetic multipole for such nuclei depends solely on the radial wave function of the valence nucleon. In fact, the spectroscopic purity remains high even for large-basis models that contain admixtures of high-lying configurations, because other configurations which could participate must be at least $2\hbar\omega$ higher in energy. If these small contributions can be neglected, the form factor of the highest magnetic multipole is further simplified because the virtual photon couples to the intrinsic spin of the valence nucleon, and not to convection currents. As a consequence of this simplicity, elastic magnetic scattering in the region of the highest multipole, i.e., $q \gtrsim 2\text{ fm}^{-1}$, has provided the most precise measurements of the radial sizes of valence nucleon orbits.^{2,3}

The description of lower magnetic multipole form factors is more complex because less stringent angular momentum requirements allow the participation of orbits other than the stretched $j = l + \frac{1}{2}$ orbit. As a result there are a number of single-particle matrix elements that can contribute, and, in general, these have different q dependences. The magnitudes of the lower multipole form factors are especially sensitive to details of the interference between the various single-particle elements. Electron scattering measurements of these magnetic multipoles therefore provide sensitive tests of calculations that go beyond the extreme single-particle shell model. Of course, for nuclei having a single nucleon outside a doubly closed core, the additional single-particle matrix elements necessarily involve nucleons in orbitals above the Fermi energy. These contributions arise from the residual nucleon-nucleon interaction.

Just two stable nuclei have one nucleon outside a doubly closed core: ^{17}O and ^{209}Bi , and of these, only the $1d_{5/2}$ neutron in ^{17}O is in the stretched configuration. The magnetic form factors of both nuclei have been measured,^{4,5} and the case of ^{17}O has especially drawn attention. The data⁴ for ^{17}O span the range $0.5 \text{ fm}^{-1} < q < 3.6 \text{ fm}^{-1}$, a region in which all the possible magnetic multipoles, $M1$, $M3$, and $M5$, make large contributions. For $q \gtrsim 2 \text{ fm}^{-1}$, where the $M5$ multipole is dominant, the data lie in good accord with the results of single-particle calculations that use radial wave functions generated from a Woods-Saxon potential well. However, in the range $q = 0.7 - 1.8 \text{ fm}^{-1}$, where the intermediate $M3$ multipole is expected to be largest, the data are considerably lower than the single-particle predictions. There have been extensive theoretical efforts to explain these data. Calculations that take CP into account produce an $M3$ suppression, but not enough to reconcile them with the data.^{6,7} Furthermore, the effects of MEC's and CP at high q , where they are expected to be important due to the rapid falloff of the one-body form factor, seem to be insignificant.⁴ This might be due to second-order CP contributions, which according to a calculation by Blunden and Castel,⁶ almost cancel those from pionic exchange currents at high q .

In this paper we report extensive measurements of the magnetic form factor of ^{41}Ca , where, according to the simple shell model, the valence neutron occupies the stretched $1f_{7/2}$ orbit outside the doubly closed ^{40}Ca core. The magnetic elastic form factor of ^{41}Ca was recently measured in the momentum transfer range $q = 1.8 - 3.3 \text{ fm}^{-1}$, a region where the highest $M7$ multipole dominates.⁸ These measurements, which were made at an angle of 155° , could not be extended to lower momentum transfers because charge scattering becomes much larger than magnetic scattering. The experiment reported in this paper was performed near 180° , where the charge cross section is at least 400 times smaller than that in 155° measurements at the same q . As a result, we were able to determine the magnetic form factor of ^{41}Ca in the q region where the $M3$ and $M5$ multipoles are dominant.

In the interpretation of the data, we have performed calculations that include multiparticle-multipole configurations in the $1f_{7/2}$ and $1d_{3/2}$ subshells, core polarization, and meson-exchange currents. As will be shown, the main effect is predicted to come from CP,

which was evaluated in first-order perturbation theory for all possible 1p-1h excitations. The inclusion of CP and configuration mixing in the $1d_{3/2}$ and $1f_{7/2}$ orbitals leads to a reduction in the magnitude of all multipoles, especially $M3$ and $M5$. In contrast, MEC's increase the calculated form factors for all multipoles.

The availability of the new data and theoretical calculations have enabled us to refine the rms size deduced for the $1f_{7/2}$ neutron orbit. Precise measurements of the radii of valence orbits are of fundamental importance for testing various models, such as mean-field theories. In addition, the size of the valence orbit in ^{41}Ca is of particular relevance to the Coulomb energy difference anomaly.⁹⁻¹¹ Binding energy differences between mirror nuclei with the same doubly closed core should be largely determined by the electromagnetic interactions of the valence nucleons. However, Coulomb energy differences calculated from such analyses are systematically smaller than the experimental values. A study by Negele¹⁰ showed that the binding energy difference between ^{41}Ca and ^{41}Sc could be explained if the radius of the $1f_{7/2}$ orbit in ^{41}Ca was 3.45 fm, a value about 15% lower than that given by mean-field calculations.

II. EXPERIMENTAL METHOD AND RESULTS

The experiment was performed at the MIT-Bates Linear Accelerator Center using the four-magnet 180° scattering system¹² in conjunction with a dispersion-matching transport system and a high-resolution, energy-loss spectrometer system.¹³ The target was a 7 mm diameter tablet of calcium carbonate (CaCO_3) of thickness 33.7 mg/cm^2 , isotopically enriched to 81.7% in ^{41}Ca . Thus the corresponding ^{41}Ca thickness was 11.2 mg/cm^2 . This radioactive target material, which has a half-life of $(1.03 \pm 0.04) \times 10^5 \text{ yr}$, was prepared at the Oak Ridge High-Flux Isotope Reactor by neutron irradiation of ^{40}Ca , with subsequent mass separation. It was contained between two thin aluminum foils of 2.5 mg/cm^2 total thickness. To avoid thermal damage to the target, the beam current was limited to $5 \mu\text{A}$.

Due to the small diameter of the target, it was essential that the beam be focused to a small spot on the center of the target. The position of the beam on the target was monitored by means of a small split-foil secondary-emission monitor mounted directly on the target frame.

TABLE I. Measured elastic magnetic cross sections and deduced form factors.

E_i (MeV)	q_{eff} (fm^{-1})	$d\sigma/d\Omega$ (mb/sr)	F_M^2	Error (%)
190.0	1.990	3.44×10^{-7}	1.93×10^{-4}	11
175.0	1.841	4.64×10^{-7}	2.20×10^{-4}	12
158.4	1.670	4.79×10^{-7}	1.86×10^{-4}	13
145.1	1.527	5.45×10^{-7}	1.77×10^{-4}	9
130.0	1.379	6.11×10^{-7}	1.60×10^{-4}	10
115.2	1.239	6.19×10^{-7}	1.27×10^{-4}	10
105.4	1.132	6.75×10^{-7}	1.16×10^{-4}	16
96.0	1.036	9.83×10^{-7}	1.40×10^{-4}	21
84.9	0.919	11.39×10^{-7}	1.27×10^{-4}	47

The foils of this monitor consisted of thin graphite so that, by virtue of nuclear recoil differences, electrons scattering from the foils were well separated in energy from those elastically scattered from ^{41}Ca . Consequently, the presence of the secondary-emission monitor did not constitute a source of background.

The elastically scattered electrons were measured for nine incident energies ranging from 85 to 190 MeV. As indicated in Table I, this corresponds to a range in momentum transfer of 0.92 to 1.99 fm^{-1} . Figure 1 shows the spectrum of scattered electrons for an incident energy of 145 MeV. Cross sections were determined by a standard line-shape-fitting procedure, and the normalization of the data was established to $\pm 3\%$ by measuring cross sections for elastic scattering from ^1H . For this purpose a 47.3 mg/cm^2 thick disk of rotating polyethylene (CH_2) was used. In addition, a small ^7Li target was mounted concentrically on the rear of the ^{41}Ca target for simultaneous measurement of the elastic cross section of ^7Li . This information was used to confirm the normalization of the data.

In the plane-wave first Born approximation, the cross section for electron scattering can be written in terms of longitudinal and transverse form factors F_L and F_T :¹

$$\frac{d\sigma}{d\Omega} = 4\pi\eta\sigma_M \left[|F_L(q^2)|^2 + \left[\frac{1}{2} + \tan^2 \frac{\theta}{2} \right] |F_T(q^2)|^2 \right],$$

where

$$\eta = \left[1 + (2E_i/M_t)\sin^2 \frac{\theta}{2} \right]^{-1}$$

is a recoil factor. In these equations θ is the scattering angle in the laboratory, E_i is the incident electron energy, and M_t is the mass of the target nucleus. The Mott cross section

$$\sigma_M = \alpha^2 \cos^2 \frac{\theta}{2} / 4E_i^2 \sin^4 \frac{\theta}{2}$$

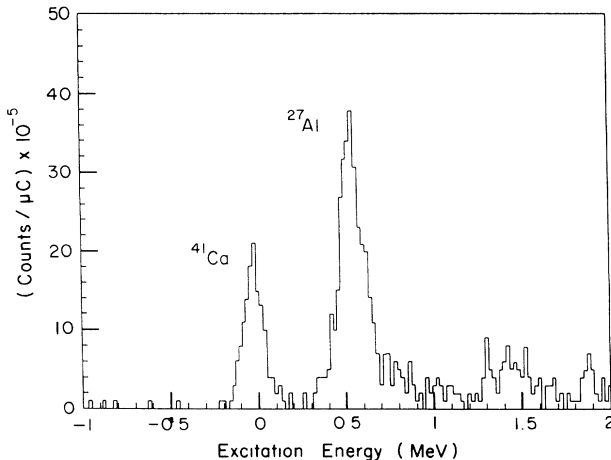


FIG. 1. Spectrum measured at $E_i = 145$ MeV for electron scattering from a $^{41}\text{CaCO}_3$ target contained between Al foils.

is for scattering from a pointlike charge, $\alpha = \frac{1}{137}$ is the fine structure constant, and

$$q^2 \approx 4E_i^2 \eta \sin^2 \frac{\theta}{2}$$

is the square of the three-momentum transfer. The transverse form factor is $F_T^2 = F_E^2 + F_M^2$, where F_E is the electric form factor which vanishes for elastic scattering, and F_M is the magnetic form factor.

For a target nucleus with ground-state angular momentum $J \neq 0$, the form factors can be written as an incoherent sum over multipoles. In elastic electron scattering from ^{41}Ca , with spin parity of $J^\pi = \frac{7}{2}^-$, the Coulomb multipoles $C0$, $C2$, $C4$, and $C6$ contribute to the longitudinal form factor, and magnetic multipoles $M1$, $M3$, $M5$, and $M7$ contribute to the transverse form factor. Whereas the longitudinal and transverse form factors can be separated experimentally, the individual multipoles cannot be isolated in a model-independent way unless polarization observables are measured. However, the multipoles have different dependences on momentum transfer which may be utilized, to some extent, to deduce the individual multipole contributions to the magnetic form factor. When, as in the present case, the scattering takes place near the nuclear surface, the lowest multipole is the most important at low q , and form factors of increasing multipolarity peak at progressively larger values of q .

In principle, the transverse form factor can be determined by measuring at $\theta = 180^\circ$, where only its contribution to the cross section remains. However, because of the finite solid angle acceptance of the spectrometer and multiple scattering in the target, longitudinal scattering from the nuclear charge distribution also contributes to the measured cross sections. This contribution, which was reduced by partially closing the spectrometer slits, was subtracted from the cross sections measured for the four lowest beam energies ≤ 115 MeV. The charge scattering cross section $(d\sigma/d\Omega)_{^{41}\text{Ca}}^L$ for ^{41}Ca is not known, but has been evaluated for the four lowest beam energies by means of

$$\left(\frac{d\sigma}{d\Omega} \right)_{^{41}\text{Ca}}^L = \left(\frac{d\sigma}{d\Omega} \right)_{^{40}\text{Ca}}^L \frac{(d\sigma/d\Omega)_{^{41}\text{Ca}}^{\text{MF}}}{(d\sigma/d\Omega)_{^{40}\text{Ca}}^{\text{MF}}},$$

where $(d\sigma/d\Omega)_{^{40}\text{Ca}}^L$ is the charge scattering cross section from ^{40}Ca , and $(d\sigma/d\Omega)_{^{41}\text{Ca}}^{\text{MF}}$ and $(d\sigma/d\Omega)_{^{40}\text{Ca}}^{\text{MF}}$ are mean-field predictions for these cross sections. A phase-shift code was utilized to compute the $(d\sigma/d\Omega)_{^{40}\text{Ca}}^L$ cross sections at the effective scattering angles,¹⁴ which ranged from 178.5° to 179.1° . These calculations were based on a parametrization¹⁵ of the ^{40}Ca charge density which accurately reproduces elastic cross sections measured for ^{40}Ca . The theoretical cross sections were determined using the Hartree-Fock-Bogoliubov formalism by Dechargé and Gogny.¹⁶ For the measurement at the lowest q the Coulomb contribution was about 27% of the total cross section, and for the other three data points it was less than 8%. In the subtraction of the charge cross section,

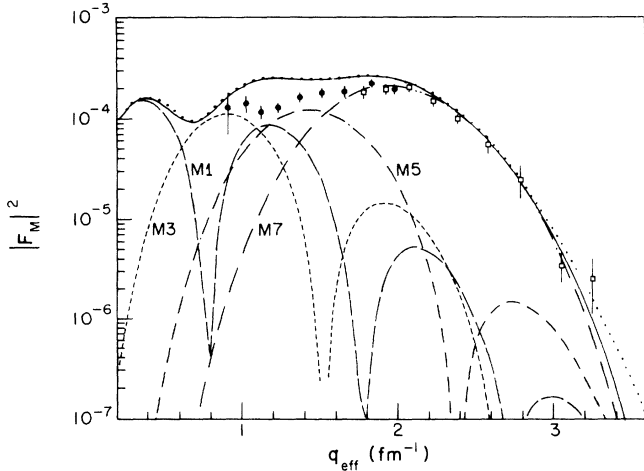


FIG. 2. The ^{41}Ca magnetic form factor data of this work (circles) and of Platchkov *et al.* (Ref. 8) (open squares) plotted vs q_{eff} . The solid and dotted curves show the total form factors calculated for Woods-Saxon and harmonic-oscillator potentials, respectively. Other curves show the individual multipoles for the Woods-Saxon potential: $M1$ (long dashed), $M3$ (dashed), $M5$ (dash-dotted), and $M7$ (dash-dot-dotted).

a 20% uncertainty was assigned to the calculated value of $(d\sigma/d\Omega)_{^{41}\text{Ca}}^{\text{mag}}$.

The square of the elastic magnetic form factor at 180° is defined by

$$|F_M(q)|^2 = \frac{(d\sigma/d\Omega)^{\text{mag}}}{4\pi\eta(\alpha/2E_i)^2},$$

where $(d\sigma/d\Omega)^{\text{mag}}$ is the magnetic cross section. The results are presented in Fig. 2 and Table I as a function of the "effective" momentum transfer q_{eff} , which includes a correction for the main effect of Coulomb distortion, an energy shift due to the attraction of the incident electron in the electric field of the nucleus. As a consequence of this attraction, the experimental cross sections are displaced towards high q . The code HADES (Ref. 17) was employed to calculate the shift in momentum transfer for the kinematics of our experiment. Figure 2 also shows previous data from Platchkov *et al.*⁸ Excellent consistency is obtained in the region of overlap with the present results.

III. INTERPRETATION AND COMPARISON WITH THEORY

In Fig. 2 the experimental data are compared with the predictions of the extreme single-particle shell model obtained using both harmonic-oscillator ($b = 1.84$ fm) and Woods-Saxon wave functions. The depth of the Woods-Saxon well, 53.3 MeV, was chosen to reproduce the 8.36-MeV binding energy of the valence neutron in ^{41}Ca . The radius and diffuseness of the well were set at $1.25(A-1)^{1/3}$ fm and 0.65 fm, respectively, and the spin-orbit potential parameter was assumed to be 6.0 MeV. For both wave functions, finite nucleon size was incorporated by the form factor f_n , for which we used the four-pole fit of Simon *et al.*,¹⁸ and center-of-mass motion was taken into account by using the harmonic-oscillator center-of-mass correction $f_{\text{c.m.}} = \exp(b^2q^2/4A)$. As can be seen in Fig. 2, there is little difference between the results obtained from the two wave functions.

Above $q = 2$ fm $^{-1}$, a region where the $M7$ multipole is dominant, the shell-model predictions agree with the data. However, at lower q the data begin to fall below the calculations, indicating that the $M3$ and $M5$ multipole contributions are suppressed (quenched) relative to the single-particle predictions. In order to assess the quenching or spectroscopic factors for these multipoles, as well as the rms radius of the $1f_{7/2}$ neutron orbital, the data were fitted by the expression

$$|F_M|^2 = \sum_{L=1, \text{odd}}^7 \alpha_L^2 |F_{ML}|^2 f_{\text{c.m.}}^2(q^2) f_n^2(q^2).$$

The free parameters in this fit were the radius of the Woods-Saxon potential well used to compute magnetic multipoles $|F_{ML}|^2$, and the quenching factors α_L of the amplitudes of the $M3$, $M5$, and $M7$ multipoles. Because no data exist in the low- q region where the $M1$ component dominates, α_1 was fixed to the value implied by the quenching of the ^{41}Ca magnetic dipole moment relative the free neutron moment: $\alpha_1 = (\mu_{^{41}\text{Ca}}/\mu_n) = 0.834$.

Figure 3 and Table II show the results of this analysis. The $1f_{7/2}$ rms radius corresponding to the fit is 3.99 ± 0.05 fm and the $M7$ quenching factor is found to be $\alpha_7 = 0.95 \pm 0.03$. These results agree with those obtained from previous magnetic scattering measurements⁸ on ^{41}Ca , 3.95 ± 0.06 fm and $\alpha_7 = 0.92 \pm 0.05$. In addition, the extracted radius is identical to that obtained³ from (e, e') data for the $1f_{7/2}$ neutron radius in ^{49}Ti : 3.99 ± 0.05 fm.

TABLE II. rms radius and quenching factors extracted for the $1f_{7/2}$ orbit, and spectroscopic factors obtained from theoretical calculations that consider core polarization (CP) and the configuration-mixed shell model (CMSM).

	rms (fm)	α_3	α_5	α_7
Uncorrected	3.99 ± 0.05	0.57 ± 0.16	0.68 ± 0.07	0.95 ± 0.03
MEC corrected	4.03 ± 0.05	0.46 ± 0.19	0.58 ± 0.07	0.84 ± 0.03
MEC+CP corrected	3.96 ± 0.05			
CP calculation		0.52	0.73	0.94
CMSM plus CP calculation		0.45	0.67	0.86

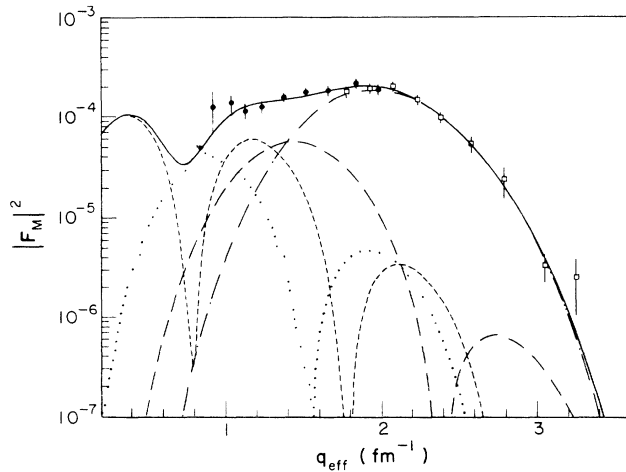


FIG. 3. Results of least-square fit to the measured ^{41}Ca elastic magnetic form factor using Woods-Saxon wave functions. The solid curve shows the total fitted form factor. Other curves show the individual multipole components: $M1$ (dashed), $M3$ (dotted), $M5$ (dash-dotted), and $M7$ (dash-dot-dotted).

The closeness to unity of the value deduced for α_7 supports arguments that the effects of core polarization from higher-lying shells are small in the case of the highest multipole, and that the extracted radius does indeed characterize the $1f_{7/2}$ orbit.

Additional analyses were performed to assess the model dependence of these results. For example, when the spin-orbit potential was raised by 1.0 MeV, the value deduced for the rms orbit size decreased by about 0.03%. Changing the diffuseness parameter a by ± 0.05 fm modified the rms radius by $\pm 0.5\%$. Both of these modifications lie well within the uncertainty assigned to the extracted $1f_{7/2}$ radius. The data were also fitted with harmonic-oscillator wave functions to examine the sensitivity of the results to the radial shape of the $1f_{7/2}$ wave function. A value of $b = 1.84$ fm was obtained for the oscillator size parameter, corresponding to a $1f_{7/2}$ radius of 3.91 ± 0.05 fm. Although the harmonic-oscillator potential is unrealistic at large radii, this result differs by only 2% from the preferred Woods-Saxon result. The results obtained for the quenching factors, $\alpha_3 = 0.56 \pm 0.16$, $\alpha_5 = 0.67 \pm 0.07$, and $\alpha_7 = 0.94 \pm 0.03$, are almost unchanged from the Woods-Saxon values indicated in Table II.

The results of the analysis prove to be more sensitive to the magnitude of the second diffraction maximum of the $M1$ form factor, which, as seen in Figs. 2 and 3, is calculated to be large in the vicinity of $q = 1.25 \text{ fm}^{-1}$. Evaluations of magnetic dipole form factors in other nuclei indicate that the magnitudes of the second diffraction maxima have considerable model dependence. In order to estimate the effects of this sensitivity, two quite extreme limits were considered. For the single-particle value $\alpha_1 = 1.0$, we obtained $\alpha_3 = 0.34 \pm 0.29$, $\alpha_5 = 0.58 \pm 0.09$, $\alpha_7 = 0.97 \pm 0.03$, and an rms size of 4.00 ± 0.05 fm. On the other hand, when the $M1$ form factor was assumed to be

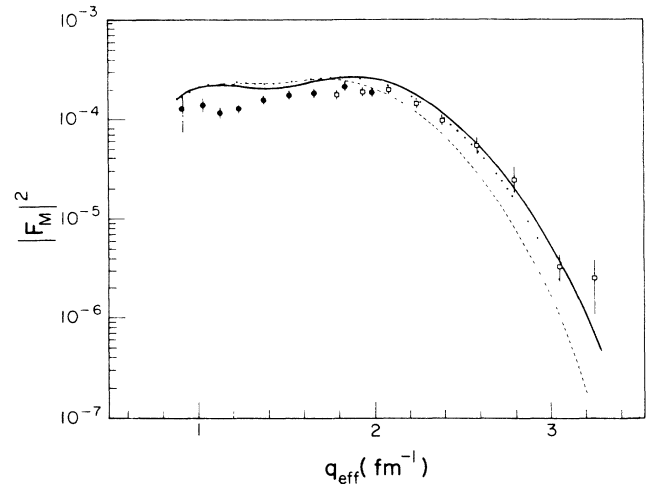


FIG. 4. Comparison of measured magnetic form factor to mean-field predictions of Dechargé and Gogny (Ref. 16) (solid line), Negele and Vautherin (Ref. 19) (dashed), and the relativistic calculation of Kim (Ref. 20) (dotted).

zero for $q > 0.8 \text{ fm}^{-1}$, the results were $\alpha_3 = 0.90 \pm 0.10$, $\alpha_5 = 0.86 \pm 0.06$, $\alpha_7 = 0.91 \pm 0.03$, and an $1f_{7/2}$ radius of 3.96 ± 0.05 fm. Although the results for α_5 , and especially α_3 , indicate appreciable model dependence, it remains clear that both of these multipoles are quenched relative to the values predicted by the single-particle model. On the other hand, the values obtained for α_7 and the rms orbital size show little sensitivity to the assumed $M1$ form factor.

In Fig. 4 the data are compared to the results of Hartree-Fock calculations by Dechargé and Gogny,¹⁶ Negele and Vautherin,¹⁹ and Kim.²⁰ The last of these calculations was performed within the relativistic mean-field framework by Serot and Walecka.²¹ At the highest momentum transfers the prediction of Negele and Vautherin decrease too rapidly, a result of the larger radial extent of the corresponding wave function. At the maximum of the $M7$ multipole, at $q \approx 2 \text{ fm}^{-1}$, there exists relatively good agreement between all three calculations and the data. Because these theories do not include configuration mixing, this agreement further supports the assumption that the properties of ^{41}Ca are largely determined by an unpaired neutron in the valence $1f_{7/2}$ orbit. However, at momentum transfers below 2 fm^{-1} , where the intermediate $M3$ and $M5$ multipoles are dominant, all calculations exceed the data. As will be demonstrated below, this is attributable to the neglect of configuration mixing.

The effects of core polarization and meson-exchange currents were evaluated within a harmonic-oscillator basis with the size parameter $b = 1.84$ fm. Core-polarization contributions were calculated by first-order perturbation theory using the Green's-function method,²² with all possible $1p$ - $1h$ configurations being included without truncation. The finite-range $M3Y$ residual interaction,²³ which contains tensor components, was used.

MEC calculations were made of one-pion, pair, and Δ -isobar currents.²⁴ Figure 5 shows how the results of the harmonic-oscillator single-particle calculations are modified by the inclusion of CP and MEC's. Core polarization has the larger effect, particularly with regard to the magnitudes of the $M3$ and $M5$ form factors, which are reduced considerably from the single-particle values. The predicted form factors are increased by the calculations of the pair and pionic exchange current diagrams, and decreased by Δ -isobar currents. Throughout the q range of the existing data, the net effect of the MEC contributions, which increases slowly with q , is to enhance the calculated magnetic form factor by 16–25%. Overall, these calculations lead to an improved theoretical understanding of the data, although, as can be seen in Fig. 5, some discrepancies still remain.

The contribution from the first-order core polarization to the magnetic dipole moment is zero, and the inclusion of MEC's raises its magnitude from the Schmidt value $-1.91\mu_N$ to $-1.99\mu_N$. This value is 20% greater than the measured dipole moment, $-1.595\mu_N$. More detailed calculations of the dipole moment, by Towner and Khanna²⁵ and Arima *et al.*,²⁶ show that second-order CP reduces the moment considerably; however, this is almost offset by a large MEC correction, much of which is associated with the CP configurations. The overall results of these calculations, $-1.91\mu_N$ and $-1.79\mu_N$, still leave a clear discrepancy with the observed $M1$ moment.

In order to isolate the part of the quenching which is due mainly to configuration mixing, we have refitted the data after subtracting the calculated MEC contributions. The results for the quenching factors, shown in Table II, are to be compared with the predicted quenching due to first-order CP alone: 0.52, 0.73, and 0.94 at the maxima of the $M3$, $M5$, and $M7$ form factors, respectively. For

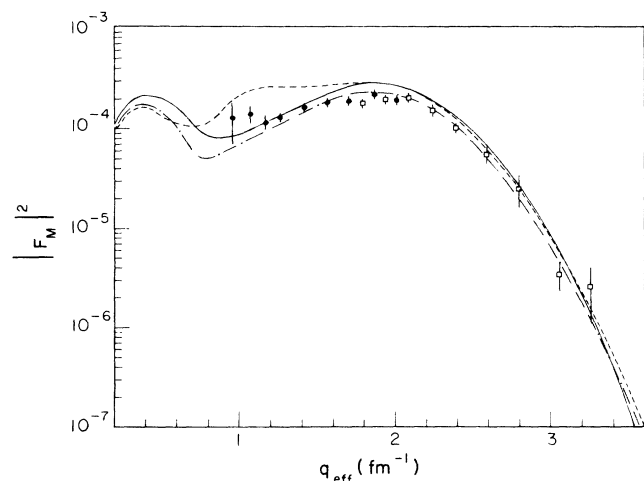


FIG. 5. Comparison of measured magnetic form factor to calculations that include first-order CP and MEC's. The dashed curve is the single-particle harmonic-oscillator result ($b = 1.84$ fm). The dash-dotted curve includes core polarization using the $M3Y$ interaction (Ref. 23), and the solid curve includes, in addition, MEC's.

the $M3$ multipole, the agreement is good. On the other hand, the experimentally deduced amplitudes for the $M5$ and $M7$ multipoles are 21% and 11% smaller than the predicted CP values.

The failure of the first-order CP calculations to give sufficient quenching of the $M5$ and $M7$ multipoles can be attributed to several factors. There is, for example, some sensitivity to the choice of the residual interaction, particularly with regard to the strength of the tensor force which is important in determining the coupling to high-lying configurations. Furthermore, the first-order CP calculations cannot fully describe the correlations that result from the nucleon-nucleon interaction. A direct consequence of these correlations is the depletion of the occupation probability of orbitals below the Fermi energy, and corresponding partial increase in the occupancy of orbitals that, in the simple shell model, are empty or sparsely populated. While the importance of correlations has been increasingly recognized, the magnitude of the effects of correlations remains an open question. For nuclei in the region of ^{208}Pb , correlations are credited^{27,28} for reducing the strengths of single-particle excitations by about 30%.

The existence of correlations in ^{40}Ca has long been recognized. One of the earliest theoretical evaluations, made by Agassi, Gillet, and Lambros²⁹ using the random phase approximation formalism, predicted that the ground state of ^{40}Ca contained, on the average, 0.8 protons and 0.8 neutrons in the $1f_{7/2}$ subshell. The second-order perturbation approach of Adachi, Lipparini, and van Gai,³⁰ which included 2p-2h configurations up to virtual excitation energies of $8\hbar\omega$, found that on the average 3.2 nucleons are excited out of the doubly magic $A = 40$ core, and that one of these nucleons occupies a $1f_{7/2}$ orbit. Similar calculations for protons by Takayanagi,³¹ who extended the model space to include 2p-2h configurations up to $26\hbar\omega$, suggest that as many as 5.65 protons lie outside the ^{40}Ca core. A different approach was taken by Mahaux and Sartor,³² who used a dispersion relation to extrapolate n - ^{40}Ca and p - ^{40}Ca scattering results to determine the nuclear mean field for negative nucleon energies. The calculated field includes a dispersive correction due to the coupling of the nucleon to excitations of the ^{40}Ca core. This calculation gives 2.1 nucleons in $1f_{7/2}$ orbitals, and 0.7 nucleon in the $2p_{3/2}$ subshell.³³ Finally, shell-model calculations were performed for Ca isotopes by Hsieh *et al.*³⁴ who distributed $A - 32$ particles without restriction in the $1d_{3/2}$ and $1f_{7/2}$ orbits. The most disturbing omissions from this model space are the $2s_{1/2}$ orbit, which lies only 1 MeV below the $1d_{3/2}$ orbit, and the $2p_{3/2}$ orbit, which lies only 2 MeV above the $1f_{7/2}$ orbit. In this calculation the ground-state occupancy of $1f_{7/2}$ subshell was determined to be 0.64 to 1.0 nucleon, depending on the assumed interaction.

Although the quantitative predictions of these various calculations deviate somewhat, experimental results support the general notion of partial occupancy of the $1f_{7/2}$ subshell in the ^{40}Ca ground state. For example, proton pickup measurements by Doll *et al.*³⁵ suggest that 0.58 proton occupy $1f_{7/2}$ orbits in the ^{40}Ca ground state. More recent ($e, e'p$) studies by Kramer^{33,36} give an occu-

pancy of 0.91 for $1f_{7/2}$ proton orbitals in ^{40}Ca . Nevertheless, neither of these results includes possible $1f_{7/2}$ strength residing in highly excited levels. Kramer³⁶ has estimated that such contributions could increase the $1f_{7/2}$ occupation probability to 3.0 protons.

On both theoretical and experimental grounds, it is apparent then that, even in ^{40}Ca , there is appreciable occupancy of the $1f_{7/2}$ subshell. It is therefore to be expected that the $1f_{7/2}$ subshell of ^{41}Ca will, on the average, be occupied by more than a single neutron. In order to evaluate the effect of such correlations the configuration-mixed shell-model calculations of Hsieh *et al.*³⁴ were repeated for ^{40}Ca and ^{41}Ca . With the “ df_i ” Hamiltonian³⁴ the following intensities were obtained for multiparticle-multihole configurations in ^{40}Ca : 72.2% 0p-0h, 24.1% 2p-2h, 3.5% 4p-4h, and 0.2% 6p-6h. For ^{41}Ca the corresponding intensities are 71.5% 1p-0h, 25.0% 3p-2h, 3.4% 5p-4h, and 0.2% 7p-6h. The average occupancy of the $1f_{7/2}$ subshell in ^{40}Ca is 0.64 nucleon and 1.65 nucleons in ^{41}Ca . Thus, according to this model, the nucleus ^{41}Ca is well represented by the weak coupling of a $1f_{7/2}$ neutron to ^{40}Ca .

One-body density matrices derived from the configuration-mixed shell-model calculation were utilized to compute the magnetic form factor of ^{41}Ca , which is shown in Fig. 6. Except for the $M1$ multipole, the result is about 13% less than the single-particle prediction, and is seen to lie in better agreement with the data. In the case of the $M7$ multipole the reduction from the single-particle prediction arises from the expansion of the model space to include configurations which cannot be coupled by an $M7$ operator.

As indicated in Fig. 6, we have also combined the configuration-mixed shell-model results with the first-order CP and MEC evaluations. Because the CP and MEC evaluations are based on the extreme harmonic-oscillator single-particle picture rather than a

configuration-mixed model, this procedure is not formally correct. Nevertheless, the resultant error should be small. The combination of the $1d_{3/2}$ - $1f_{7/2}$ configuration mixing, CP to higher-excited orbits, and MEC's yields the best theoretical description of the data. As indicated in the last row of Table II, the quenching of the $M3$, $M5$, and $M7$ multipoles, due to the $1d_{3/2}$ - $1f_{7/2}$ configuration mixing and first-order CP, is close to that deduced from MEC-corrected experimental results. Any remaining differences can be assigned to admixtures of configurations that lie outside the model space considered here.

MEC and CP contributions, especially those in the vicinity of the $M7$ multipole, also influence the value of the extracted $1f_{7/2}$ orbital radius. The theoretical calculations have again been relied upon to correct the deduced size for such effects. The results of our analyses show that although these corrections are very small, roughly 1%, the precise values obtained for the corrections depend upon the particular prescription chosen for their evaluation. Platchkov *et al.*³ have assessed MEC corrections by fitting pseudodata generated from various theoretical calculations. In this way it was found that the rms sizes deduced for valence $1f_{7/2}$ orbits in ^{49}Ti and ^{51}V were increased by 1.4% when MEC contributions were removed. For ^{41}Ca this procedure leads to a 0.4% increase in the $1f_{7/2}$ orbital size. We have also evaluated the MEC correction by refitting the data after subtracting theoretical MEC contributions, calculated using harmonic-oscillator wave functions with $b = 1.84$ fm, the value which best describes the data. In this case the correction was 1.0%, giving an rms size equal to 4.03 ± 0.05 fm. The correction for CP has the opposite sign to the MEC correction, and when both effects were considered, a value of 3.96 ± 0.05 fm was deduced for the $1f_{7/2}$ radial size, with the indicated 1.3% error arising solely from statistical uncertainties. The uncertainty associated with the theory-derived MEC and CP corrections is difficult to assess, but, given the smallness of these corrections, is likely to be comparable to the statistical uncertainty. Sub-Coulomb heavy-ion transfer reactions have also been used to determine the rms radius of the $1f_{7/2}$ orbit in ^{41}Ca . These measurements^{37,38} give 4.00 ± 0.06 fm and 3.89 ± 0.12 fm, values that are in good agreement with the present result.

The $1f_{7/2}$ neutron orbit size is also in reasonable agreement with the mean-field predictions of 4.02 fm and 4.05 fm obtained by Dechargé and Gogny¹⁶ and by Kim,²⁰ whereas the prediction of Negele and Vautherin,¹⁹ 4.14 fm, is about 4.5% too large. The ^{41}Ca results are therefore in accord with results³ obtained for other $1f_{7/2}$ -shell nuclei, ^{49}Ti and ^{51}V , as well as the $1g_{9/2}$ -shell nuclei ^{87}Sr and ^{93}Nb . In each of these cases, the rms sizes of the valence orbits deduced from high- q electron scattering measurements are in agreement with those predicted by Dechargé and Gogny. On the other hand, the observed radius of the $1f_{7/2}$ orbit is about 15% greater than the value needed¹⁰ to resolve the Coulomb energy difference anomaly between ^{41}Ca and ^{41}Sc .

In summary, the measured magnetic form factor for ^{41}Ca shows a suppression relative to the single-particle

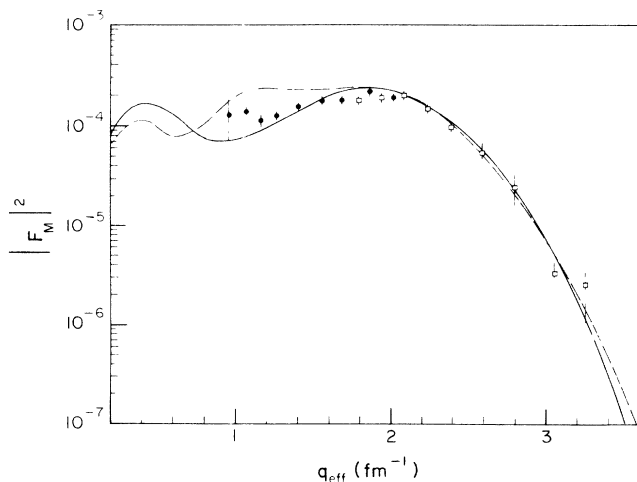


FIG. 6. The dashed curve is the result of a shell-model calculation that assumes nine nucleons to be distributed without restriction in the $1d_{3/2}$ and $1f_{7/2}$ orbits. The solid curve also includes first-order CP and MEC corrections.

shell model in the region $1 \leq q \leq 2 \text{ fm}^{-1}$, particularly where the $M3$ and $M5$ form factors are dominant. Although the respective deduced quenching factors, $\alpha_3 = 0.57 \pm 0.16$ and $\alpha_5 = 0.68 \pm 0.07$, show some model dependence, both multipoles are clearly quenched relative to single-particle model predictions. The quenching factor deduced for the $M7$ multipole, $\alpha_7 = 0.95 \pm 0.03$, has little model sensitivity. Calculations show that MEC's increase the magnetic form factor by roughly 20% for all multipoles. Subtraction of the calculated MEC contributions further reduces the quenching factors. The experimentally observed quenching can be largely explained by multiparticle-multihole configurations in the $1f_{7/2}$ and $1d_{3/2}$ orbitals, and first-order CP involving higher-excited shells. The largest effect is obtained for the $M3$ and $M5$ multipoles. Overall, the predicted quenching of the $M3$, $M5$, and $M7$ multipoles is in reasonable agreement with the data. Small lingering discrepancies would likely be accounted for by an expansion of the model space to include configurations other than those considered here.

The rms size deduced for the $1f_{7/2}$ neutron orbit lies within 1% of the corresponding sizes found by Platchkov *et al.*³ for the $1f_{7/2}$ neutron orbit in ^{49}Ti and the $1f_{7/2}$

proton orbit in ^{51}V . This finding is in accord with the predictions of mean-field calculations.¹⁶ When MEC and CP contributions are taken into account, the rms radius of the $1f_{7/2}$ neutron orbit in ^{41}Ca was determined to be $3.96 \pm 0.05 \text{ fm}$. This value is consistent with the results of sub-Coulomb transfer measurements, which, in contrast to the present result, are sensitive to the radial shape of the assumed wave functions. The deduced radial size also agrees with the mean-field predictions of Dechargé and Gogny,¹⁶ and rules out the small radius required to resolve the Coulomb energy difference anomaly.

ACKNOWLEDGMENTS

The authors are grateful to J. Dechargé, M. Girod, E. J. Kim, and J. W. Negele for providing us with mean-field wave functions, and to J. Dubach for shell-model calculations. This work was supported by the U.S. Department of Energy under Grants DE-FG02-88ER40415 and DE-AC05-84OR21400, the latter with Martin Marietta Energy System, Inc.; by National Science Foundation under Contract No. NSF PHY 86-10493; and by a grant under the Monbusho International Scientific Research Program.

*Present address: Department of Physics, University of Washington, Seattle, WA 98195.

†Present address: IHEP, Academia Sinica, P.O. Box 918, Beijing, People's Republic of China.

‡Present address: Stanford Linear Accelerator Center, Stanford, CA 94309.

¹T. W. Donnelly and I. Sick, *Rev. Mod. Phys.* **56**, 461 (1984); T. W. Donnelly and J. D. Walecka, *Nucl. Phys. A* **201**, 81 (1973).

²I. Sick, *Comments Nucl. Part. Phys.* **9**, 55 (1980).

³S. Platchkov, J. Bellicard, J. M. Cavedon, B. Frois, D. Goutte, M. Huet, P. Leconte, Phan Xuan-Xo, P. K. A. de Witt Huberts, L. Lapikás, and I. Sick, *Phys. Rev. C* **25**, 2318 (1982).

⁴N. Kalantar-Nayestanaki, H. Baghaei, W. Bertozzi, S. Dixit, J. M. Finn, C. E. Hyde-Wright, S. Kowalski, R. W. Lourie, C. P. Sargent, P. E. Ulmer, L. Weinstein, M. V. Hynes, J. J. Kelly, and B. L. Berman, *Phys. Rev. Lett.* **60**, 1707 (1988); M. V. Hynes, H. Miska, B. Norum, W. Bertozzi, S. Kowalski, F. N. Rad, C. P. Sargent, T. Sasanuma, W. Turchinetz, and B. L. Berman, *ibid.* **42**, 1444 (1979).

⁵J. R. Moreira, I. C. Nascimento, K. Arito, J. Friedrich, A. Enomoto, T. Terasama, and Y. Torizuka, *Phys. Rev. Lett.* **36**, 566 (1976).

⁶P. G. Blunden and B. Castel, *Nucl. Phys. A* **445**, 742 (1985).

⁷A. Arima, Y. Horikawa, H. Hyuga, and T. Suzuki, *Phys. Rev. Lett.* **40**, 1001 (1978); **42**, 1186 (1979).

⁸S. Platchkov, A. Amroun, P. Bricault, J. M. Cavedon, P. K. A. de Witt Huberts, P. Dreux, B. Frois, C. D. Goodman, D. Goutte, J. Martino, V. Meot, G. A. Peterson, X. H. Phan, S. Raman, and I. Sick, *Phys. Rev. Lett.* **61**, 1465 (1988).

⁹J. A. Nolen, Jr. and J. P. Schiffer, *Annu. Rev. Nucl. Sci.* **9**, 471 (1969); *Phys. Lett.* **29B**, 396 (1969).

¹⁰J. W. Negele, *Nucl. Phys. A* **165**, 305 (1971).

¹¹S. Shlomo, *Rep. Prog. Phys.* **A41**, 957 (1978).

¹²G. A. Peterson, J. B. Flanz, D. V. Webb, H. de Vries, and C.

Williamson, *Nucl. Instrum. Methods* **160**, 375 (1979).

¹³W. Bertozzi, M. V. Hynes, C. P. Sargent, C. Creswell, P. C. Dunn, A. Hirsch, M. Leitch, B. Norum, F. N. Rad, and T. Sasanuma, *Nucl. Instrum. Methods* **141**, 457 (1977); W. Bertozzi, M. V. Hynes, C. P. Sargent, W. Turchinetz, and C. Williamson, *ibid.* **162**, 211 (1979).

¹⁴R. E. Rand, *Nucl. Instrum. Methods* **39**, 45 (1966).

¹⁵I. Sick, J. B. Bellicard, J. M. Cavedon, B. Frois, M. Huet, P. Leconte, P. X. Ho, and S. K. Platchkov, *Phys. Lett.* **88B**, 245 (1979).

¹⁶J. Dechargé and D. Gogny, *Phys. Rev. C* **21**, 1568 (1980).

¹⁷H. G. Andresen, M. Engel, M. Müller, and H. J. Ohlbach, *Nucl. Phys. A* **358**, 365c (1981).

¹⁸G. G. Simon, C. Schmitt, F. Borkowski, and V. H. Walther, *Nucl. Phys. A* **333**, 381 (1980).

¹⁹J. W. Negele and D. Vautherin, *Phys. Rev. C* **5**, 1472 (1972); and private communication.

²⁰E. J. Kim, Ph.D. thesis, Stanford University, 1987; and private communication.

²¹B. D. Serot and J. D. Walecka, *Adv. Nucl. Phys.* **16**, 1 (1986).

²²T. Suzuki, M. Oka, H. Hyuga, and A. Arima, *Phys. Rev. C* **26**, 750 (1982).

²³G. Bertsch, J. Borysowicz, H. McManus, and W. G. Love, *Nucl. Phys. A* **284**, 399 (1977).

²⁴T. Suzuki and H. Hyuga, *Nucl. Phys. A* **402**, 491 (1983).

²⁵I. S. Towner and F. C. Khanna, *Nucl. Phys. A* **399**, 344 (1983).

²⁶A. Arima, K. Shimizu, W. Bentz, and H. Hyuga, in *Advances in Nuclear Physics*, edited by J. W. Negele and Erich Vogt (Plenum, New York, 1987), Vol. 18.

²⁷V. Pandharipande, C. N. Papanicolas, and J. Wambach, *Phys. Rev. Lett.* **53**, 1133 (1984).

²⁸C. N. Papanicolas, L. S. Cardman, J. H. Heisenberg, O. Schwentker, T. E. Milliman, F. W. Hersman, R. S. Hicks, G. A. Peterson, J. S. McCarthy, J. Wise, and B. Frois, *Phys.*

- Rev. Lett. **58**, 2296 (1987).
- ²⁹D. Agassi, V. Gillet, and A. Lambroso, Nucl. Phys. **A130**, 129 (1969).
- ³⁰S. Adachi, E. Lipparini, and Nguyen van Gai, Nucl. Phys. **A438**, 1 (1985).
- ³¹K. Takayanagi, Phys. Lett. B **233**, 271 (1989).
- ³²C. Mahaux and R. Sartor, Nucl. Phys. **A484**, 205 (1988).
- ³³G. J. Kramer, H. P. Blok, J. F. J. van den Brand, H. J. Bulten, E. Jans, J. B. J. M. Lanen, L. Lapikas, H. Nann, E. N. M. Quint, G. van der Steenhoven, P. K. A. de Witt Huberts, and G. J. Wagner Phys. Lett. B **227**, 199 (1989).
- ³⁴S. T. Hsieh, X. Ji, R. Mooy, and B. H. Wildenthal, in *Nuclear Structure at High Spin, Excitation, and Momentum Transfer* (McCormick's Creek State Park, Bloomington, Indiana), Proceedings of the Workshop on Nuclear Structure at High Spin, Excitation, and Momentum Transfer, AIP Proc. No. 142, edited by Hermann Nann (AIP, New York, 1985), p. 357.
- ³⁵P. Doll, G. J. Wagner, K. T. Knöpfle, and G. Mairle, Nucl. Phys. **A263**, 210 (1976).
- ³⁶G. J. Kramer, Ph.D. dissertation, University of Amsterdam, 1990.
- ³⁷J. L. Durell, C. A. Harter, J. N. Mo, and N. R. Phillips, Nucl. Phys. **A334**, 144 (1980).
- ³⁸G. D. Jones, J. L. Durell, and N. R. Phillips, Nucl. Phys. **A230**, 173 (1974).